Exploring the microstructure and tensile properties of cold-rolled low and medium carbon steels after ultrafast heating and quenching

Castro Cerda, F. M.; Schulz, B.; Celentano, D.; Monsalve, A.; Sabirov, I.; Petrov, R. H.

DOI
10.1016/j.msea.2018.12.036

Publication date
2019

Document Version
Final published version

Published in
Materials Science and Engineering A

Citation (APA)
Castro Cerda, F. M., Schulz, B., Celentano, D., Monsalve, A., Sabirov, I., & Petrov, R. H. (2019). Exploring the microstructure and tensile properties of cold-rolled low and medium carbon steels after ultrafast heating and quenching. *Materials Science and Engineering A*, *745*, 509-516. https://doi.org/10.1016/j.msea.2018.12.036

Materials Science & Engineering A 745 (2019) 509–516

Contents lists available at ScienceDirect

Materials Science & Engineering A

journal homepage: www.elsevier.com/locate/msea

Exploring the microstructure and tensile properties of cold-rolled low and medium carbon steels after ultrafast heating and quenching

F.M. Castro Cerda[a,*], B. Schulz[a], D. Celentano[b], A. Monsalve[a], I. Sabirov[c], R.H. Petrov[d,e]

[a] Department of Metallurgy, University of Santiago de Chile, Alameda Libertador Bdo. O'Higgins 3363, Estación Central, 9170022 Santiago, Chile
[b] Departamento de Ingeniería Mecánica y Metalúrgica, Centro de Investigación en Nanotecnología y Materiales Avanzados (CIEN-UC), Pontificia Universidad Católica de Chile, Vicuña Mackenna 4860, Macul, 7820436, Santiago, Chile
[c] IMDEA Materials Institute, Calle Eric Kandel 2, Getafe, 28906 Madrid, Spain
[d] Department of Electrical Energy Metals, Mechanical constructions & Systems, Ghent University, Technologiepark 903, 9052 Gent, Belgium
[e] Department of Materials Science and Engineering, Delft University of Technology, Mekelweg 2, 2628 CD Delft, The Netherlands

ARTICLE INFO

Keywords:
Ultrafast heating
Steel
Martensite
Mechanical properties

ABSTRACT

The aim of the present study is to evaluate the impact of heating rate on the microstructure and tensile properties of cold-rolled low and medium carbon steels. For this purpose, cold-rolled low and medium carbon steels were subjected to short peak-annealing experiments at 900 and 1100 °C under three heating rates (10, 450 and 1500 °C/s). The microstructure reveals a mixture of phases and microconstituents (ferrite, bainite, and as-quenched martensite) which are related to the carbon heterogeneities in austenite. The microstructural characterization suggests that the grain refinement achieved after ultrafast heating has a minor effect on the yield and ultimate tensile strength, compared to the relative microstructural distribution. It is suggested that the interplay of various strengthening mechanisms in samples subjected to ultrafast heating rates are responsible for the observed increase in strength and ductility.

1. Introduction

The application of ultrafast (> 100 °C/s) heating rates to cold-rolled low carbon steel has been subject of recent studies [1–6] due to the variety of microstructures and mechanical properties which can be obtained. The formation of austenite during continuous heating can be accomplished either under carbon diffusion or interface controlled mechanism, depending on the heating rate and local chemical composition. The combination of ultrafast heating rates and quenching without soaking time (peak-annealing experiments) results in the formation of martensite with a range of carbon contents, bainite and retained austenite. This is a consequence of the inhomogeneous carbon distribution during the peak annealing experiments.

The effect of heating rate on mechanical properties of cold-rolled low carbon steels has previously been investigated elsewhere [2,7–11]. It was found that the increase of the heating rate produces an increment in both strength and ductility due to the microstructure-refinement effect of rapid heating rates. In the majority of such studies, however, fast heating experiments were combined with prolonged holding stages at the peak temperature [8,9,11]. The disadvantage of such an approach lays on the grain growth and coarsening which takes place during isothermal annealing, thus eliminating the refinement achieved by fast heating rates [12].

Ultrafast anisothermal peak-annealing experiments [2,7,10] (i.e. continuous heating at constant heating rates to the peak temperature followed by quenching) have yielded improved mechanical performance on steels as compared with conventional heating rates (< 10 °C/s). For example, in previous studies [2,7], the average increase in yield strength was ~200 MPa. In these experiments, the holding time was below 0.5 s (except in [10] which was 2 s and the increase in strength was ~40 MPa). Although the previous results have been reported for steels with a low content of alloying elements, peak-annealing experiments can be applied to explore the resulting mechanical properties of lean materials, such as low and medium carbon steels.

The main objective of the present work is to study the effect of heating rate on microstructure and tensile properties of cold-rolled low and medium carbon steels. The constitution of austenite transformation products was assessed via in-depth microstructural characterization. The grain diameter distribution was determined by means of orientation-imaging microscopy based on the electron backscatter diffraction technique.

* Corresponding author.
E-mail address: felipe.castro@usach.cl (F.M. Castro Cerda).

https://doi.org/10.1016/j.msea.2018.12.036
Received 9 August 2018; Received in revised form 7 December 2018; Accepted 10 December 2018
Available online 17 December 2018

Table 1
Chemical composition (in wt%) of the studied steels.

Steel	C	Mn	Si	Cu	Fe
0.2%C	0.17	1.08	0.22	0.27	Bal.
0.45%C	0.44	0.63	0.26	0.23	Bal.

Table 2
Hot-rolling parameters.

Reheating Temp, °C	No. of passes	Finishing Temp, °C	Cooling
1150	6	900	Air

2. Materials and experimental procedures

2.1. Materials and applied heat-treatments

The chemical composition of the materials used in this study is shown in Table 1. Two steel bars of 0.2% and 0.45% C were purchased in the as-rolled condition. Rectangular specimens of $100 \times 32 \times 40\ mm^3$ were cut and hot-rolled in several passes to a final thickness of 4 mm. The parameters of hot-rolling are listed in Table 2. The 4 mm thickness hot-rolled sheets of 0.2% and 0.45% C were 75% cold-rolled. Fig. 1a shows the microstructure of samples after hot-rolling (Fig. 1a, b) and cold-rolling (Fig. 1c, d). Rectangular samples of $200 \times 12 \times 1\ mm^3$ were cut for heat treatments. The length of the samples was kept parallel to the rolling direction (RD) of the steel sheet. The heating experiments were carried out in the Gleeble 3800 thermomechanical simulator at heating rates of 10, 450 and 1500 °C/s to the peak annealing temperatures of 900 and 1100 °C with the soaking time of ~0.1 s. The water quenching was applied with the cooling rate of ~−3000 °C/s. The temperature was controlled by a K-type thermocouple spot welded to the midsection of each specimen. Additional thermocouples were attached to the samples at 5 mm distance from the sample center in order to control the temperature variations within 5 °C. The length of the homogeneously heat-treated zone was investigated via optical microscopy and Vickers hardness measurements. In all samples, its length was at least 12 mm.

2.2. Microstructural characterization

The microstructure was investigated using Optical Microscopy (OM), Scanning Electron Microscopy (SEM), and Electron Backscatter Diffraction (EBSD) techniques. The characterization was performed on the TD plane (the plane which is normal to the sample transverse direction) at the center of the heat-treated zone, where the controlling thermocouple was welded. Metallographic samples were prepared according to the standard procedure by grinding and polishing to 1 μm diamond paste. The microstructure was revealed by etching with a solution of 4% HNO_3 in ethanol (Nital 4%) for ~10 s at room temperature. EBSD measurements were performed after additional mechanical polishing for 40 min using colloidal silica with a particle size of 35 nm. EBSD characterization was performed with a FEI Quanta™ 450-FEG-SEM operated at 20 kV, beam current of 2.3 nA (corresponding to FEI spot size 5 for aperture 30 μm) and a working distance of 16 mm. The sample was 70° tilted towards the EBSD detector, and the EBSD patterns were acquired on a hexagonal scan grid with a lateral step size of 0.1 μm and detected by a Hikari detector operated with EDAX-TSL-

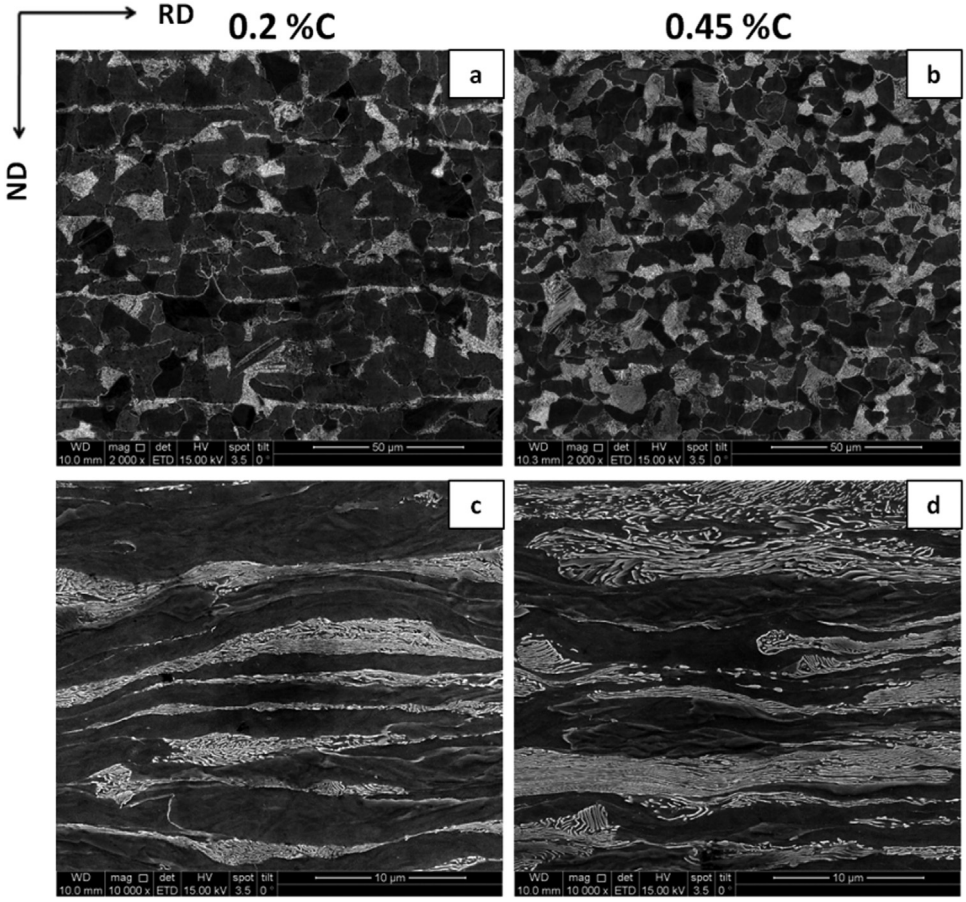

Fig. 1. Microstructure of the hot-rolled (a, b) and cold-rolled (c, d) steels. Left-hand side images correspond to 0.2%C steel, whereas right-hand side to 0.45%C steel. Etched with Nital 4%. Scalebar 50 μm (a, b) and 10 μm (c,d).

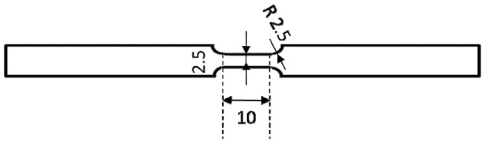

Fig. 2. Geometry of tensile specimens.

OIM-Data Collection, version 6 software. The grains were defined as the arrangement of at least 4 points with a misorientation angle above 5° and confidence index above 0.1. Grain diameter was estimated as the equivalent circular diameter of the detected grain in the EBSD map under the above grain definition. The martensitic grain diameter is measured as the average of the grain diameters in the microstructure, and it might contain also small fractions of bainite and ferrite.

2.3. Tensile tests

Three sub-size tensile specimens were cut for each heat treated condition. The geometry and dimensions of the samples are shown in Fig. 2. The selection of such geometry was related to the small size of the homogeneously heat treated area in the specimens (see Section 2.1). The cross-head speed was 1 mm/min. The axis of the specimens was parallel to the rolling direction (RD) of the sheet. The strain was measured using an extensometer. The yield strength (YS) was determined as the conventional 0.2% offset, whereas the uniform elongation (UE) was determined at the ultimate tensile strength (UTS).

3. Results

3.1. Microstructure

The initial 75% cold-rolled microstructure is shown in Fig. 1c,d. In both steels, it consists of deformed ferrite and pearlite. The OM images of microstructures after heat treatments are shown in Fig. 3. The left-hand side in each image of Fig. 3 illustrates the microstructure of 0.2%C steel heated at 10 °C/s (a, d), 450 °C/s (b, e) and 1500 °C/s (c, f) to 900 °C (a, b and c) and 1100 °C (d, e and f). It is observed that the martensitic microstructure in samples heated at 10 °C/s is finer at 900 °C peak temperature compared to the sample heated at 10 °C/s to 1100 °C, which is a reasonable consequence of the smaller Parent Austenitic Grain Size (PAGS) in the former. Samples heated at 10 °C/s (cf. Fig. 3a, d) have a fully homogeneous martensitic microstructure, while samples heated at ≥450 °C/s to 900 °C show a rather heterogeneous distribution of fine-grained martensite (cf. M arrows in Fig. 3b, c) and bainite (cf. M+B arrows in Fig. 3b, c). In samples heated at heating rates ≥450 °C/s to 1100 °C, the mixture of martensite and bainite is also observed (cf. M+B arrows in Fig. 3e, f). Likewise, the images in the right-hand side of Fig. 3 denote the microstructure of 0.45%C steel heated at 10 °C/s (a, d), 450 °C/s (b, e) and 1500 °C/s (c, f) to 900 °C (a, b and c) and 1100 °C (d, e and f). As in the 0.2%C steel, the martensitic microstructure in samples heated at 10 °C/s to 900 °C/s (cf. Fig. 3a) is finer than in samples heated to 1100 °C (cf. Fig. 3d). Samples heated at a heating rate ≥450 °C/s to 900 °C show a mixture of martensite and bainite (arrows in Fig. 3b, c) in well-defined zones of the microstructure. Such dark gray areas are also observed in all samples heated to 1100 °C (cf. Fig. 3d–f).

Fig. 4 shows SEM images of the 0.2% and 0.45%C steel samples heated to 900 °C. The upper and lower rows on the figure denotes the microstructure of 0.2%C and 0.45%C steel, respectively. Besides the mixture of martensite and bainite observed in all conditions, the presence of small ferritic grains in the 0.2%C steel (cf. F arrow in Fig. 4a–c) should be noted. These grains are located at the Parent Austenitic Grain (PAG) boundaries and were not resolved via OM. In the 0.45%C steel samples, small ferritic grains were also observed (cf. Fig. 4e,f). Some few undissolved cementite (cf. dashed circles in Fig. 4) were observed in all 0.45%C steel samples. The microstructures described hitherto are in good agreement with the previous study on a hot-rolled UFH steel

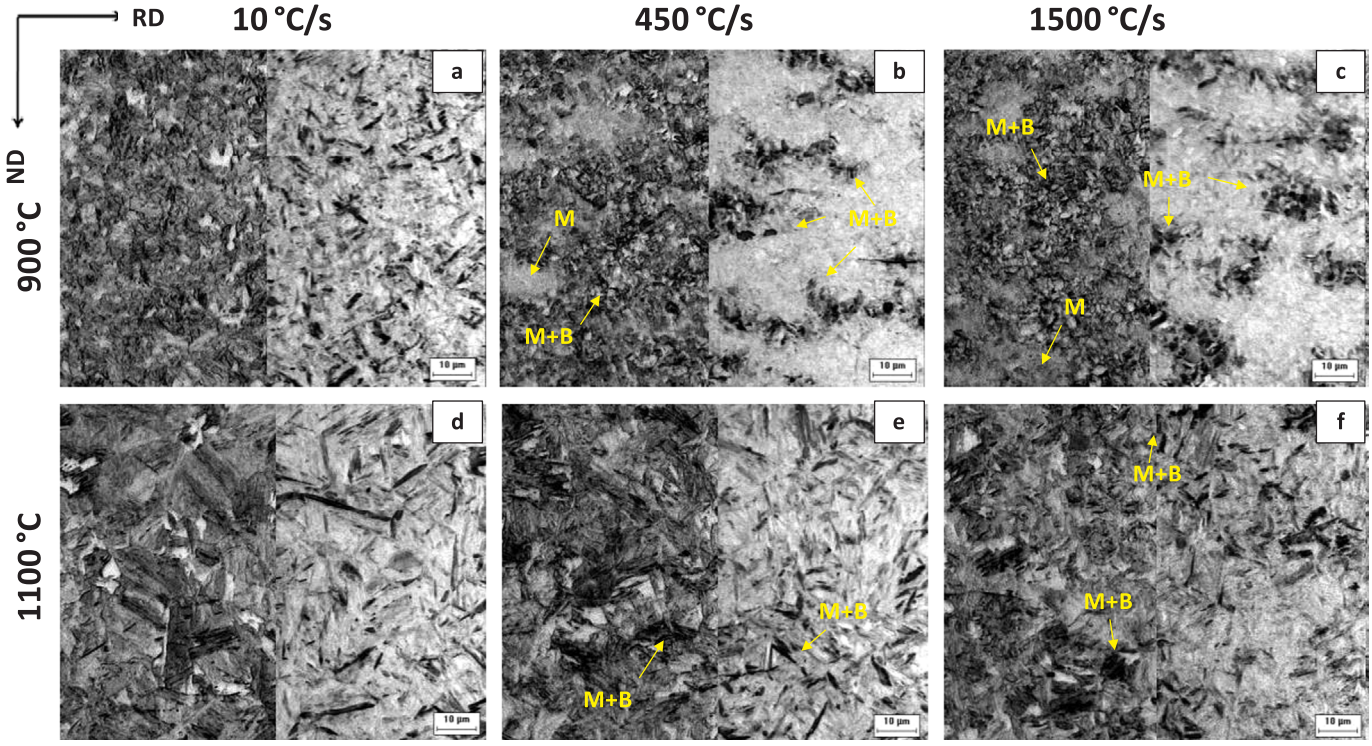

Fig. 3. OM images of the 0.2%C and 0.45%C steels heated at 10, 450 and 1500 °C/s (left-hand, center and right-hand side, respectively) to the peak temperature of 900 °C (a, b, and c) and 1100 °C (d, e, and f). The left-hand side of each image shows the microstructure of 0.2%C steel, whereas the right-hand side shows the microstructure of 0.45%C steel. The microstructure consists of martensite (light gray) and bainite (black). Etched with Nital 4%, scale bar 10 µm.

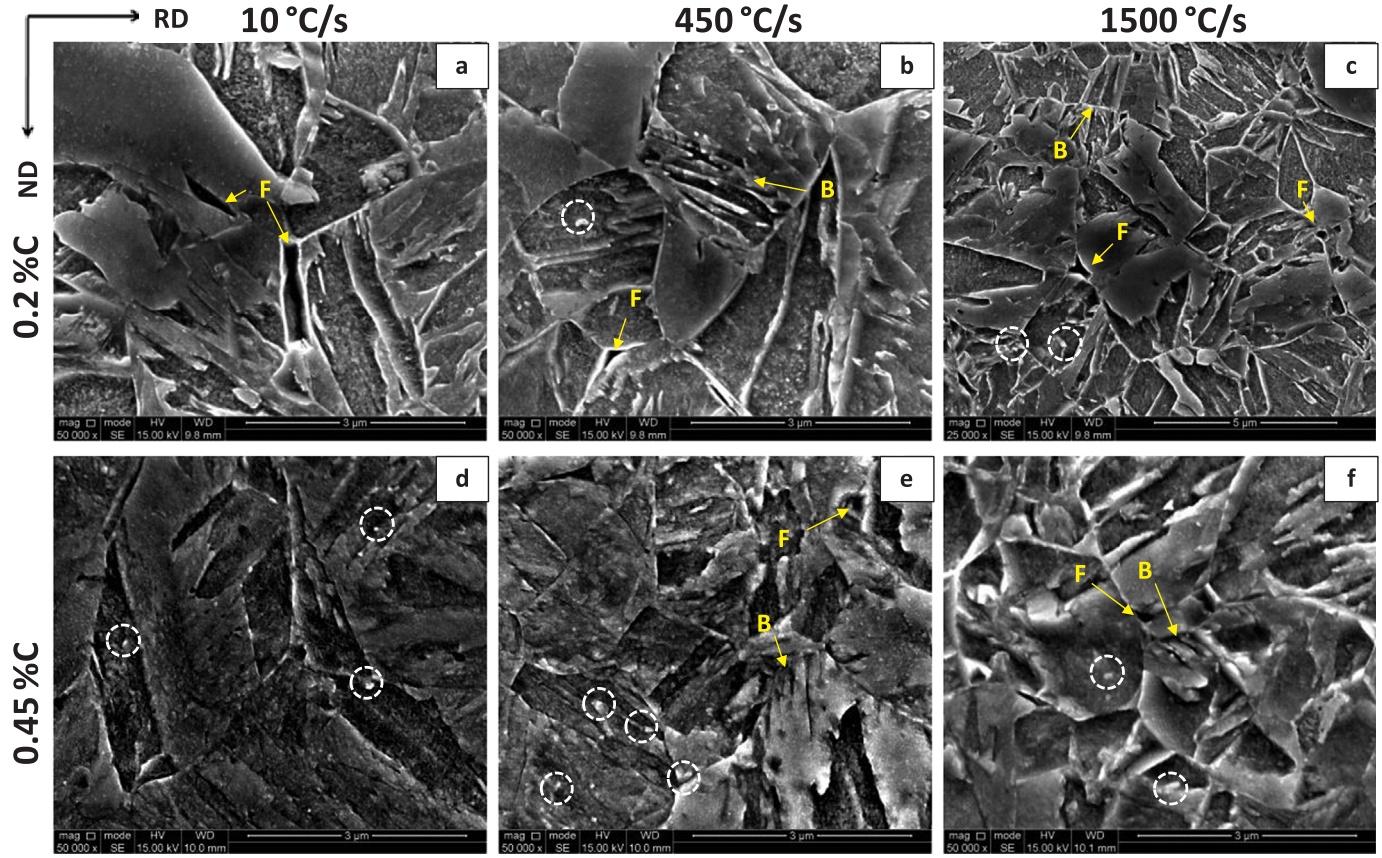

Fig. 4. SEM images of 0.2%C and 0.45%C steel heated at 10, 450 and 1500 °C/s to the peak temperature of 900 °C. The upper row (a, b, c) shows the microstructure of 0.2%C steel, whereas the lower (d, e, f) shows the microstructure of 0.45%C steel. The microstructure consists of martensite (M) and bainite (B), ferrite (F) and undissolved cementite (dashed circles). Etched with Nital 4%, scale bar 5 μm.

with a similar chemical composition [13].

The dependence of average martensitic grain diameter (AMGD) with the heating rate was calculated via EBSD data, and is shown in Fig. 5. As the heating rate increases, the AMGD does not show a noticeable variation in samples heated to 900 °C (cf. yellow bars in Figs. 5, ~2 μm), regardless the initial chemical composition. The same is observed in the 0.45%C steel samples heated to 1100 °C (cf. blue bars in Figs. 5b, ~4 μm). In samples heated to 1100 °C (cf. blue bars in Fig. 5a), there is a decrease in the average diameter with increasing heating rate. However, such decrease extends to a value comparable to the average diameter of the 0.45%C steel samples. Fig. 5 also shows the variation of the maximum martensitic grain diameter (MMGD) with the heating rate, where yellow-filled triangles and blue-filled circles show data of 900 and 1100 °C peak temperature, respectively. The calculation was done on each EBSD scan using the methodology proposed by Gomes and Kestens [14]. The maximum diameters follow relatively similar variations with respect to the AMGD. In samples heated to 900 °C, the maximum diameters oscillate around ~6 μm (cf. yellow-filled triangles in Fig. 5a, b). The same description applies to the 0.45%C steel heated to 1100 °C (cf. blue-filled circles in Fig. 5b).

3.2. Mechanical properties

Fig. 6 shows the engineering stress-strain curves measured for each thermal condition. The 0.45%C steel samples heated at 10 °C/s to 1100 °C could not be tested because they fractured after the heat treatment. It should be pointed out that the 0.45%C steel samples after heat-treatment showed very low ductility until the UTS, therefore the

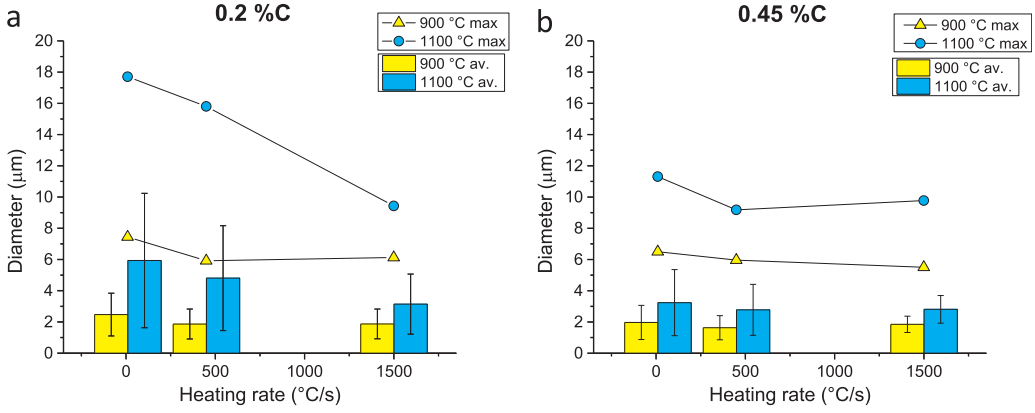

Fig. 5. EBSD-based data on the variation of equivalent circular martensitic diameter with the heating rate in the 0.2%C (a) and 0.45%C (b) steel samples. Yellow and blue bars show the average martensitic grain diameter (AMGD) of samples heated to 900 and 1100 °C, respectively. Yellow-filled triangles and blue-filled circles show the maximum martensite grain diameter (MMGD) of samples heated to 900 and 1100 °C, respectively (For interpretation of the references to color in this figure legend, the reader is referred to the web version of this article).

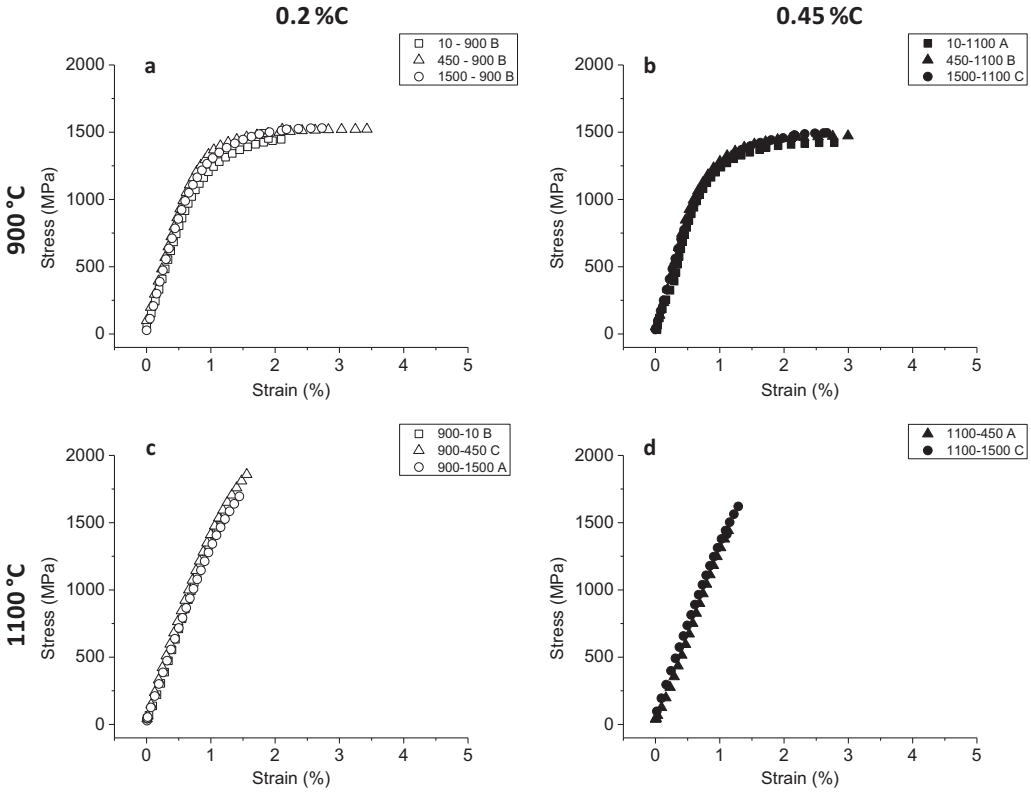

Fig. 6. Engineering stress-strain curves of the 0.2%C (a, b) and 0.45%C (c, d) steel samples. Outlined figures show the curves of samples treated to 900 °C peak temperature (a, c), whereas filled figures (b, d) displays the curves of samples treated to 1100 °C.

Table 3
Mechanical properties of the heat treated steels.

0.2%C Steel								
HR,	**900 °C**							
°C/s	**YS, MPa**	**SD**	**UTS, MPa**	**SD**	**UE, %**	**SD**	**U_T**	**SD**
10	1284	8	1500	0	2.1	0.4	60	4
450	1227	65	1504	50	2.6	0.7	64	4
1500	1164	37	1519	50	2.4	0.5	64	12
	1100 °C							
10	1232	45	1428	56	2.2	0.5	47	17
450	1111	31	1486	15	3	0.1	50	10
1500	1037	63	1445	71	2.8	0.8	51	15
0.45%C Steel								
HR,	**900 °C**							
°C/s	**YS, MPa**	**SD**	**UTS, MPa**	**SD**	**UE, %**	**SD**	**U_T**	**SD**
10	–	–	1606	41	1.3	0	11	1
450	1661	57	1886	6	1.1	0	23	11
1500	1593	16	1736	40	1.1	0	18	7
	1100 °C							
10	–	–	–	–	–	–	–	–
450	–	–	1303	239	1.1	0	11	3
1500	–	–	1698	27	1	0	15	5

0.2% offset strength could not be measured. Fig. 6a, b illustrates the curves of the 0.2%C steel samples, whereas Fig. 6c, d shows the curves of the 0.45%C steel samples. It is seen that the uniform elongation of the 0.2%C steel samples is between 2% and 3.5%. The 0.45%C steel samples fail without significant plastic deformation (i.e., < 1% of elongation to fracture). A summary of the mechanical properties is presented in Table 3.

4. Discussion

4.1. Continuous austenite formation

The thermodynamics and kinetics of continuous austenite formation in low and medium carbon steels of ferrite plus pearlite initial microstructure have been recently described [13]. The present discussion considers some particular aspects of the previous reference.

4.1.1. Formation of austenite

Let us consider a ferrite-pearlite aggregate which is heated at a constant rate. The nucleation of austenite will take place at the α/θ interface at certain temperature above the critical A_1 [13]. Therefore, the nucleus can grow either towards ferrite or cementite. The growth of austenite in either case is controlled by carbon diffusion. Two possible paths can be readily identified during austenite growth in a ferrite-pearlite aggregate: (i) towards pearlite and (ii) towards proeutectoid ferrite. The distance for carbon diffusion in austenite growing into pearlite is a factor of the interlamellar spacing [15], whereas the diffusion distance in austenite growing towards proeutectoid ferrite is increasing with time to a value $\approx d/2$, where d is the mean grain diameter of ferrite. Due to the large difference in the carbon diffusion distance (a couple of orders of magnitude), the growth of austenite towards pearlite is faster. If the heating rate is slow (< 1 °C/s) the formation of austenite is controlled by carbon diffusion. Under ultrafast heating rates (> 100 °C/s) the last stage of austenite formation is likely to be achieved by a massive mechanism. The transition temperature from the carbon diffusion control to the massive one has been referred to as A_m, and it is defined as the temperature in which $\Delta G^{\alpha\rightarrow\gamma} = 0$ when $X_C \rightarrow 0$, where $\Delta G^{\alpha\rightarrow\gamma}$: Gibbs free energy change of the austenite formation from ferrite and X_C: mole fraction of carbon [13]. The last fraction of austenite formed under ultrafast heating grows massively. Considering that the holding time at the annealing temperature is very short (0.1 s), the carbon redistribution within austenitic grains is negligible and, thus, the beginning of ferrite formation upon cooling is also likely to be massive. The lack of carbon redistribution hypothesis is supported by observation of ferrite at PAG boundaries and bainite in samples heated above 450 °C/s (cf. Fig. 5). Otherwise, austenite with homogeneously distributed carbon therein would result in martensitic

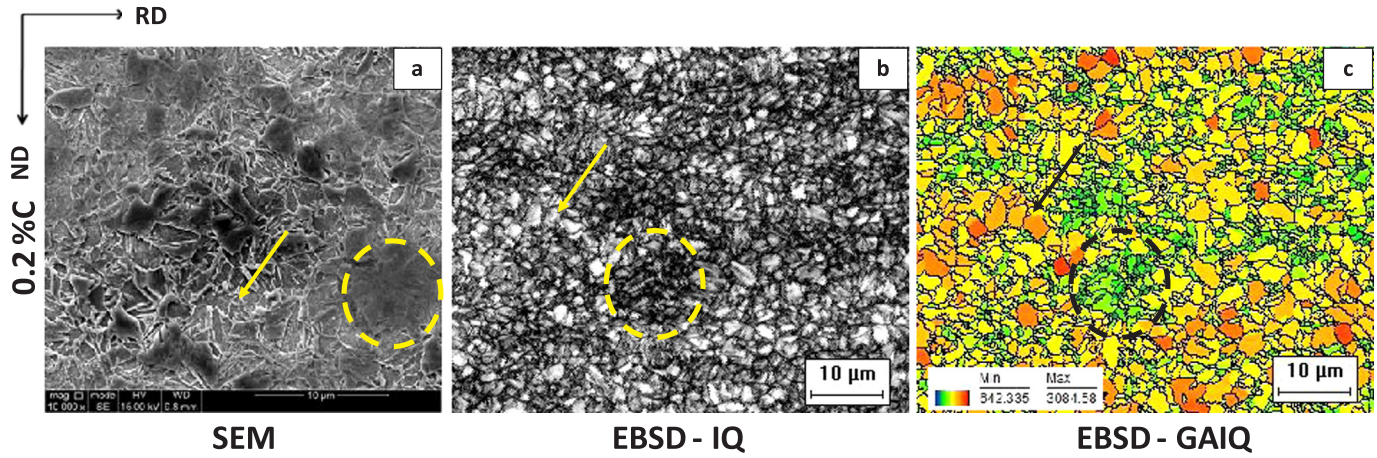

Fig. 7. Images of the 0.2%C steel heated at 1500 °C/s to the peak temperature of 900 °C. SEM, IQ and GAIQ images correspond to (a), (b) and (c), respectively, whereas high carbon martensitic areas are marked by dashed circles. The step size and scale bar on SEM images are 80 nm and 10 µm, respectively.

structure after quenching at ~-3000 °C/s.

4.1.2. Transformation products

The heterogeneous distribution of carbon in austenite will produce a distribution of transformation products during cooling. Fig. 4 shows areas of different etching response, which correspond to a distribution of ferrite, bainite and martensite. Fig. 7 shows a comparison of SEM images with EBSD IQ-based maps for samples heated at 1500 °C/s to 900 °C. IQ (Image Quality) is a parameter which is sensitive to the lattice distortion. Whereas high IQ areas (cf. light gray-white in Fig. 7b) represent zones of defect-free crystals, low IQ areas (cf. light gray-dark gray in Fig. 7b) represent zones with high concentration of defects. When combined with a suitable grain definition, IQ maps can represent the average IQ value per grain (cf. Fig. 7c). This characteristic of the IQ-based map has been applied to the phase quantification in Dual-Phase steels [7]. Although the specific areas in the images are not the same, it can be readily noticed in Fig. 7b that light-gray grains represent ferritic grains in Fig. 7a (yellow arrows). The low IQ areas are easily visualized on the Grain Average Image Quality (GAIQ) map (cf. Fig. 7c). Blue-yellow grains represent the grains with the lower average IQ, whereas red grains show grains with high average IQ. The great majority of the microstructure after heating at 1500 °C/s to 900 °C is martensite, i.e., blue-yellow grains in Fig. 7c. Hence, light gray grains in Fig. 7b (red grains in Fig. 7c) correspond to ferrite. It is noticeable that martensitic structure displays a gradient of IQ values (cf. Fig. 7b, c). Similar IQ maps showing a gradient have also been reported elsewhere [13] under ultrafast heating rates.

It is suggested that such IQ heterogeneities are product of the carbon heterogeneities in austenite. The transformation products upon cooling range from low-carbon phases and microconstituents (such as ferrite or mixtures of ferrite and bainite) to martensite. The phase distribution in the initial ferrite and pearlite microstructure suggests that the austenite quickly forms at pearlitic colonies and then grows towards proeutectoid ferrite. It is reasonable to expect that the high carbon martensite will inherit its composition from austenite nucleated at the former pearlitic colonies. One high-carbon zone has been outlined in Fig. 7 (dashed circle).

4.2. Evolution of mechanical properties

As described in Section 3.1, the microstructure resulting from ultrafast heating is a mixture of martensite, bainite, ferrite and undissolved cementite. However, the largest phase fraction corresponds to martensite. Thus, the mechanical properties predominantly depend on the characteristics of martensite. It is obvious that the largest strength and the lowest ductility will be associated with the 0.45%C samples. A slight increase of both strength and ductility in the 0.2%C samples under ultrafast heating is nevertheless observed. In the following sections, an attempt to rationalize the differences in tensile properties between samples under different thermal paths is carried out.

4.2.1. Yield strength

Table 3 shows the variation of YS and UTS versus heating rate. In the 0.2%C samples, YS slightly decreases with increasing heating rate for both peak temperatures. Conversely, in the 0.45%C samples, the YS increases as the heating rate is increased to maximum at 450 °C/s and then it slightly decreases. Although in the present study it was not possible to accurately measure the volume fractions of ferrite and bainite in the microstructure, Fig. 3 qualitatively show that there is a considerable fraction of bainite in the microstructure at heating rates ≥ 450 °C/s. The effect of the heating rate on the fraction of ferrite and bainite, as discussed in Section 4.1.2, could partially justify the continuous decrease in the YS measured in the 0.2%C samples. The presence of carbon heterogeneities in austenite will give rise, besides ferrite and bainite, to martensite with different carbon contents (cf. dashed circles in Fig. 7) and thus of different strength. The fraction of low carbon martensite in samples under UFH rates is also thought to be influencing the decrease in the YS observed in the 0.2%C samples. The behavior of the YS in the 0.45%C samples could only be determined for 450 and 1500 °C/s to 900 °C peak temperature. The relative decrease can be rationalized analogous to the 0.2%C samples. The microstructural analysis suggests that the carbon heterogeneities in austenite, resulting in strength distribution in martensite, ferrite and bainite, have the main influence on the YS of samples under UFH rates. The decrease in the AMGD (cf. blue bars in Fig. 7a) does not have an impact on the YS of the 0.2%C samples heated to 1100 °C. The AMGD is nearly constant under the other experimental conditions.

4.2.2. Ultimate tensile strength

It is thought that the UTS is mainly influenced by the strength of martensite, which is determined by its carbon content. The carbon content of austenite comes from cementite dissolution above A_1. Zener [16] proposed an expression for the isothermal growth of spherical precipitates in a supersaturated matrix, which was later adapted by Hillert [17] for representing the dissolution of cementite in austenite. For a binary Fe-C system, the velocity of the γ/θ interface $v^{\gamma/\theta}$ (m/s) can be written as

$$v^{\gamma/\theta} = \frac{D_C \, \Delta X_C}{r^{\theta}(X_C^{\theta} - X_C^{\gamma})} \quad (1)$$

where D_C: diffusivity of carbon in austenite (m^2/s), ΔX_C: is the difference of carbon in austenite (mole fraction), r_θ: initial radius of cementite (m), X_C^k: mole fraction of C in the phase k. Microstructural observation showed traces of undissolved cementite in the 0.45%C samples heated at ≥450 °C/s. Since the pearlitic structure is quite similar in both initial microstructures, it is reasonable to expect that cementite is not fully dissolved as well in the 0.2%C samples heated at ≥450 °C/s. It is clear that both ΔX_C and (X_C^θ - X_C^γ) terms increase with temperature, which predicts that the dissolution of cementite should be larger in the samples heated to 1100 °C. The increase of the heating rate implies a shortening of the time range between austenite formation beginning and peak temperature. Therefore, it is reasonable to expect that the largest cementite dissolution will be found at the lowest heating rate, i.e., 10 °C/s. Based on the kinetics of cementite dissolution and carbon enrichment in austenite, one should expect finding the largest UTS values in the samples heated at 10 °C/s to 1100 °C. Conversely, the comparatively lower hardenability of austenite formed under UFH rates promotes the formation of bainite, which might further decrease the strength.

From examination of Table 3 it is seen that the UTS does not show a noticeable variation with the peak temperature. It was measured an increase in the UTS in both samples heated to 900 and 1100 °C peak temperatures, contrary to what it should be expected from the contribution of cementite dissolution in austenite. The simplest explanation for the lowest UTS value under 10 °C/s is the presence of microcracks due to martensitic transformation, as a consequence of the very fast cooling rates. It can be hypothesized that under UFH rates the strain accommodation of high-carbon martensite zones might be assisted by the softer low-carbon martensite, bainite and ferritic grains. The UTS of the 0.45%C samples heated to 900 °C (cf. Table 3) shows an increase of ~280 MPa with increasing heating rate from 10 to 450°C/s. With further increasing heating rate to 1500 °C/s, the UTS drops by ~150 MPa (still 130 ~MPa higher than in the sample heated at 10 °C/s). Carbon content in martensite is not playing the most significant role in the strengthening of martensite under the current experimental set-up due to carbon heterogeneities as discussed above. EBSD data shows that the AMGD decreases from ~6 μm to ~3 μm in the 0.2%C samples heated to 1100 °C. It could be argued that the reduction in grain diameter (cf. Fig. 5) could account for the increase (or the counter balance of the expected drop) in the UTS observed in the 0.2%C samples heated at 900 and 1100 °C according to the Hall-Petch [18,19] relationship, yet the AMGD is almost constant in the 0.2%C and 0.45%C samples heated to 900 °C (cf. Fig. 5). The possible impact of work hardening mechanism on the UTS will be discussed in Section 4.2.3.

4.2.3. Work hardening

Since the available literature dealing with the strain hardening mechanisms in microstructures generated by UFH is scarce, and the experimental concept does not consider the determination of any specific activation barrier, no attempt of estimation of individual mechanisms to the work hardening will be made. Fig. 7 shows that the work hardening is similar under the three heating rates. However, both UTS and uniform elongation are increasing with heating rate. One could thus hypothesize that, although the work hardening capacity of the structure seems to be low, the strain hardening mechanisms in samples heated at 10 °C/s are not necessarily the same as in the samples under ultrafast heating rates.

Whereas it is expected that austenite is relatively homogeneous in samples heated at 10 °C/s, the existence of carbon heterogeneities in austenite as a consequence of ultrafast heating rates suggests the existence of retained austenite (RA), as reported elsewhere [7]. Retained austenite can transform into martensite during plastic deformation (the so-called Transformation-induced plasticity, or TRIP effect), increasing the strain accommodation and the UTS thereon.

The presence of small particles of undissolved cementite, either product of incomplete pearlite dissolution of bainitic transformation, might give rise to the Zener pinning effect [20]. It is observed in Fig. 5 that the *distance* between cementite particles (white circles) is of the order of a couple of microns in the bulk and of tens of nanometers within bainite. Hence, an effective interaction between cementite and dislocation may be possible.

4.2.4. Ductility and toughness

The uniform elongation in the 0.45%C samples does not show a significant variation under the experimental conditions of the present study. The reason stems in the high carbon content of martensite which decreases the ductility. In the 0.2%C samples heated to 900 and 1100 °C, the uniform elongation slightly increases as the heating rate increases from 10 to 450 °C/s. Toughness of the materials is estimated as an area under the stress – strain curve. Qualitative analysis of the stress – strain curves presented in Table 3 shows that toughness (U_T) of the material is also to some extent affected by the heating rate. Particularly, the 0.2%C steel shows the higher values of toughness after heating with ≥450 °C/s to both peak temperatures. Somewhat lower values are calculated for the 0.45%C steel heated to 900 °C, although a slight increase is observed for heating rates ≥450 °C/s. No clear conclusion can be made for the latter steel heated to 1100 °C due to significant scatter of experimental results.

These observations can be rationalized based on the presence of microcracks in the samples heated at 10 °C/s. The observed increase in the uniform elongation and toughness under heating rates ≥450 °C/s is thought to be related to the presence of low carbon martensite, bainite and ferrite, as discussed in the previous sections. The possible contribution of retained austenite to the ductility strongly depends on the stability of retained austenite, which is beyond the scope of the present study.

5. Conclusions

Continuous heating experiments under heating rates of 10, 450 and 1500 °C/s to 900 and 1100 °C peak temperatures were carried out on the cold-rolled 0.2 and 0.45%C steel. The combined microstructural characterization and tensile tests allowed to analyze the contribution of the microstructural features resulting from ultrafast heating and quenching, such as carbon heterogeneities and the presence of proeutectoid (massive) ferrite and bainite. EBSD data are discussed under the hypothesis of carbon heterogeneities in austenite.

The heating rate variation of the average martensitic grain diameter show a very small decrease in samples heated to 900 °C (less than 1 μm) in both steels. In samples heated to 1100 °C, the decrease in average grain diameter in 0.2%C steel is ~3 μm, whereas in 0.45%C steel the variation is less than 1 μm. Fair agreement is found between the EBSD-based maximum martensitic grain diameter and the reconstructed parent austenitic grain.

The variation in the YS and UTS with the heating rate seems to correlate primarily with the qualitative increase in the fraction of ferrite and bainite. The transformation of such constituents on cooling arises from the carbon heterogeneities in austenite.

Acknowledgements

F.M. Castro Cerda acknowledges the support of Fondecyt Chile via project no. 11170104.

References

[1] T. Lolla, G. Cola, B. Narayanan, B. Alexandrov, S.S. Babu, Development of rapid heating and cooling (flash processing) process to produce advanced high strength steel microstructures, Mater. Sci. Technol. 27 (2011) 863–875, https://doi.org/10.1179/174328409x433813.

[2] D. De Knijf, A. Puype, C. Föjer, R. Petrov, The influence of ultra-fast annealing prior to quenching and partitioning on the microstructure and mechanical properties, Mater. Sci. Eng. A 627 (2015) 182–190, https://doi.org/10.1016/j.msea.2014.12.

118.
[3] C.W. Lee, W.S. Choi, Y.R. Cho, B.C. De Cooman, Direct resistance joule heating of Al-10 pct Si-coated press hardening steel, Metall. Mater. Trans. A 47 (2016) 2875–2884, https://doi.org/10.1007/s11661-016-3467-x.
[4] K. Wang, B. Zhu, L. Wang, Y. Wang, Y. Zhang, Tailored properties of hot stamping steel by resistance heating with local temperature control, Procedia Manuf. 15 (2018) 1087–1094, https://doi.org/10.1016/j.promfg.2018.07.383.
[5] I. Hordych, K. Bild, V. Boiarkin, D. Rodman, F. Nürnberger, Phase transformations in a boron-alloyed steel at high heating rates, Procedia Manuf. 15 (2018) 1062–1070, https://doi.org/10.1016/j.promfg.2018.07.386.
[6] L.S. Thomas, D.K. Matlock, Formation of banded microstructures with rapid intercritical annealing of cold-rolled sheet steel, Metall. Mater. Trans. A (2018), https://doi.org/10.1007/s11661-018-4742-9.
[7] F.M. Castro Cerda, C. Goulas, I. Sabirov, S. Papaefthymiou, A. Monsalve, R.H. Petrov, Microstructure, texture and mechanical properties in a low carbon steel after ultrafast heating, Mater. Sci. Eng. A 672 (2016) 108–120, https://doi.org/10.1016/j.msea.2016.06.056.
[8] J. Huang, W.J. Poole, M. Militzer, Austenite formation during intercritical annealing, Metall. Mater. Trans. A 35 (2004) 3363–3375, https://doi.org/10.1007/s11661-004-0173-x.
[9] D. Xu, J. Li, Q. Meng, Y. Liu, P. Li, Effect of heating rate on microstructure and mechanical properties of TRIP-aided multiphase steel, J. Alloy. Compd. 614 (2014) 94–101, https://doi.org/10.1016/j.jallcom.2014.06.075.
[10] Q. Meng, J. Li, H. Zheng, High-efficiency fast-heating annealing of a cold-rolled dual-phase steel, Mater. Des. 58 (2014) 194–197, https://doi.org/10.1016/j.matdes.2014.01.055.
[11] G. Liu, S. Zhang, J. Li, J. Wang, Q. Meng, Fast-heating for intercritical annealing of cold-rolled quenching and partitioning steel, Mater. Sci. Eng. A 669 (2016) 387–395, https://doi.org/10.1016/j.msea.2016.05.106.
[12] L.A.I. Kestens, D. De Knijf, F.M. Castro Cerda, R.H. Petrov, Advanced high strength steels: improved properties by design of textures and microstructures, IOP Conf. Ser. Mater. Sci. Eng. 219 (2017) 1–14, https://doi.org/10.1088/1757-899X/219/1/012004.
[13] F.M. Castro Cerda, I. Sabirov, C. Goulas, J. Sietsma, A. Monsalve, R.H. Petrov, Austenite formation in 0.2% C and 0.45% C steels under conventional and ultrafast heating, Mater. Des. 116 (2017) 448–460, https://doi.org/10.1016/j.matdes.2016.12.009.
[14] E. Gomes, L.A.I. Kestens, Fully automated orientation relationship calculation and prior austenite reconstruction by random walk clustering, IOP Conf. Ser. Mater. Sci. Eng. 82 (2015) 12059 http://stacks.iop.org/1757-899X/82/i=1/a=012059.
[15] G.R. Speich, A. Szirmae, Formation of austenite from ferrite and ferrite-carbide aggregates, Trans. AIME 245 (1969) 1063–1073.
[16] C. Zener, Theory of growth of spherical precipitates from solid solution, J. Appl. Phys. 20 (1949) 950–953, https://doi.org/10.1063/1.1698258.
[17] M. Hillert, K. Nilsson, L.-E. Torndahl, Effect of alloying elements on the formation of austenite and dissolution of cementite, J. Iron Steel Inst. 209 (1971) 49–66.
[18] E.O. Hall, The deformation and ageing of mild steel: III discussion of results, Proc. Phys. Soc. Sect. B 64 (1951) 747 http://stacks.iop.org/0370-1301/64/i=9/a=303.
[19] N.J. Petch, The cleavage strength of polycrystals, J. Iron Steel Inst. 174 (1953) 25–28.
[20] C.S. Smith, Grains, phases, and interfaces—an interpretation of microstructure, Trans. AIME 175 (1948) 15–51.